Nuclear Science and Techniques (2024) 35:32
https://doi.org/10.1007/s41365-024-01387-4

Investigating the elliptic anisotropy of identified particles in p–Pb collisions with a multi-phase transport model

Si-Yu Tang[1] · Liang Zheng[2] · Xiao-Ming Zhang[3] · Ren-Zhuo Wan[4,5]

Received: 21 July 2023 / Revised: 11 September 2023 / Accepted: 13 September 2023 / Published online: 28 March 2024
© The Author(s), under exclusive licence to China Science Publishing & Media Ltd. (Science Press), Shanghai Institute of Applied Physics, the Chinese Academy of Sciences, Chinese Nuclear Society 2024

Abstract

The elliptic azimuthal anisotropy coefficient (v_2) of the identified particles at midrapidity ($|\eta| < 0.8$) was investigated in p–Pb collisions at $\sqrt{s_{\mathrm{NN}}} = 5.02$ TeV using a multi-phase transport model (AMPT). The calculations of differential v_2 based on the advanced flow extraction method of light flavor hadrons (pions, kaons, protons, and Λ) in small collision systems were extended to a wider transverse momentum (p_{T}) range of up to 8 GeV/c for the first time. The string-melting version of the AMPT model provides a good description of the measured p_{T}-differential v_2 of the mesons but exhibits a slight deviation from the baryon v_2. In addition, we observed the features of mass ordering at low p_{T} and the approximate number-of-constituent-quark (NCQ) scaling at intermediate p_{T}. Moreover, we demonstrate that hadronic rescattering does not have a significant impact on v_2 in p–Pb collisions for different centrality selections, whereas partonic scattering dominates in generating the elliptic anisotropy of the final particles. This study provides further insight into the origin of collective-like behavior in small collision systems and has referential value for future measurements of azimuthal anisotropy.

Keywords Azimuthal anisotropy · Small collision systems · Transport model

1 Introduction

The main goal of heavy-ion collisions at ultrarelativistic energies is to explore the deconfined state of strongly interacting matter created at a high energy density and temperature, known as the gluon plasma (QGP) [1, 2]. An important observation for investigating the transport properties of the QGP is anisotropic flow [3, 4], which is quantified by the flow harmonic coefficients v_n obtained from the Fourier expansion of the azimuthal distribution of the produced particles [5, 6]:

$$\frac{\mathrm{d}N}{\mathrm{d}\varphi} \propto 1 + 2\sum_{n=1}^{\infty} v_n \cos[n(\varphi - \Psi_n)], \tag{1}$$

where φ is the azimuthal angle of the final-state particle angle and Ψ_n is the symmetry plane angle in the collision

This work was supported by the Key Laboratory of Quark and Lepton Physics (MOE) in Central China Normal University (Nos. QLPL2022P01, QLPL202106), Natural Science Foundation of Hubei Provincial Education Department (No. Q20131603), National key research, development program of China (No. 2018YFE0104700), National Natural Science Foundation of China (No. 12175085), Fundamental research funds for the Central Universities (No. CCNU220N003).

✉ Liang Zheng
zhengliang@cug.edu.cn

✉ Xiao-Ming Zhang
xiaoming.zhang@ccnu.edu.cn

✉ Ren-Zhuo Wan
wanrz@wtu.edu.cn

1 School of Mathematical and Physical Sciences, Wuhan Textile University, Wuhan 430200, China

2 School of Mathematics and Physics, China University of Geosciences (Wuhan), Wuhan 430074, China

3 Key Laboratory of Quark and Lepton Physics (MOE) and Institute of Particle Physics, Central China Normal University, Wuhan 430079, China

4 Hubei Key Laboratory of Digital Textile Equipment, Wuhan Textile University, Wuhan 430200, China

5 School of Electronic and Electrical Engineering, Wuhan Textile University, Wuhan 430200, China

for the n-th harmonic [7, 8]. The second-order coefficient v_2, referred to as the elliptic flow, is derived from the initial state spatial anisotropy of the almond-shaped collision overlap region that is propagated to the final state momentum space. The magnitude of the elliptic flow is sensitive to the fundamental transport properties of the fireball, such as the temperature-dependent equation of state and the ratio of shear viscosity to entropy density (η/s) [9, 10].

Over the past few decades, various measurements of elliptic flow in heavy-ion collisions performed at the relativistic heavy-ion collider (RHIC) [11–14] and the Large Hadron Collider (LHC) [15–18] have helped build a full paradigm of the strongly coupled QGP. Comprehensive measurements of p_T-differential elliptic flow of the identified particles were conducted by the ALICE Collaboration [19, 20]. The observed mass-ordering effect (i.e., heavier particles have a smaller elliptic flow than lighter particles at the same p_T) at low p_T is well described by hydrodynamic calculations and is attributed to the radial expansion of the QGP [21]. At intermediate p_T, the grouping of v_2 of mesons and baryons was observed, with mesons exhibiting less v_2 than baryons. These behaviors can be explained by the hypothesis that baryons and mesons have different production mechanisms through quark coalescence, which has been further investigated using the number-of-constituent-quark (NCQ) scaling [22–25]. Interestingly, such flow-like phenomena have been observed in small-collision systems. Long-range double-ridge structures were first measured in high-multiplicity pp and p–Pb collisions by the ALICE, ATLAS, and CMS collaborations [26–28]. The measurement of elliptic and triangular azimuthal anisotropies in central ^{3}He+Au, d+Au, and p+Au collisions performed by the STAR Collaboration [29] suggests that sub-nucleon fluctuations also play an important role in influencing the flow coefficients in these small collision systems. In addition, these measurements were extended to the identified particles associated with the discovery of a significant positive v_2 [30, 31]. The observed particle-mass dependence of v_2 is similar to that measured in heavy-ion collisions [30]; however, the origin of such collective-like behavior remains unclear. Several theoretical explanations relying on either the initial state or final state effects have been proposed to understand the origin of azimuthal anisotropies in small systems. Studies that extend hydrodynamics from large to small systems based on final-state effects can well describe v_2 of soft hadrons [32–36]; however, they are based on the strong assumption that there is sufficient scattering among constituents in small systems. Hydrodynamics combined with the linearized Boltzmann transport (LBT) model can also describe the identified particle v_2 in a high-multiplicity small-collision system at an intermediate p_T [37]. Color-glass condensate (CGC)-based models and IP-Glasma models that consider the effect of momentum correlations in the initial state can quantitatively describe some features of collectivity in p–Pb collisions [38, 39], but without clear conclusions, particularly regarding the dependence on collision systems and rapidity.

In addition, an approach called parton escape shows that few scatterings can also create sufficient azimuthal anisotropies, which have been investigated using multi-phase transport (AMPT) [40, 41]. The v_2 values of light hadrons measured in p–Pb collisions are well described in AMPT, where the contribution of anisotropic parton escape rather than hydrodynamics plays an important role [41]. In this study, we extend the AMPT calculations of the p_T-differential v_2 for identified particles ($\pi^{\pm}$, $K^{\pm}$, $p(\bar{p})$, $\Lambda(\bar{\Lambda})$) to higher p_T region in p–Pb collisions at 5.02 TeV, in order to systematically test the mass-ordering effect and baryon-meson grouping at low- and intermediate-p_T, respectively. We also investigate how the key mechanisms implemented in AMPT, such as the parton cascade and hadronic rescattering, affect elliptic anisotropy in small collision systems. In addition, various non-flow subtraction methods with different sensitivities to jet-like correlations were studied.

2 Model and methodology

2.1 A multi-phase transport model

The string-melting version of the AMPT model (v2.26t9b, available online) [40, 42] was employed in this study to calculate v_2 of the final-state particles in high-multiplicity p–Pb at 5.02 TeV. The AMPT model includes four main processes: initial conditions, partial scattering, hadronization, and hadronic interactions. The initial conditions are generated from the heavy ion jet interaction generator (HIJING) model [43, 44], where minijet partons and soft-excited strings are produced and then converted to primordial hadrons based on Lund fragmentation. Under the string-melting mechanism, primordial hadrons are converted into partons, a process determined by their flavor and spin structures. Elastic scattering between the partons was simulated using Zhang's parton cascade (ZPC) model [45], which includes two-body scattering with a cross section described by the following simplified equation:

$$\sigma_{gg} \approx \frac{9\pi\alpha_s^2}{2\mu^2}. \tag{2}$$

In this study, the strong coupling constant α_s was set to 0.33, and the Debye screening mass $\mu = 2.2814\ \mathrm{fm}^{-1}$, resulting in a total parton scattering cross section of $\sigma = 3$ mb. To isolate

Table 1 Details of three configurations

Description	σ (mb)	t_{max} (fm/c)
w/ all	3	30
w/o parton scat	~0	30
w/o hadron scat	3	0.4

the effect of partonic scattering, σ is adjusted to be close to 0 by increasing μ (see set "w/o parton scat." in Table 1). Once the partonic interaction ceases, hadronization with a quark coalescence model is implemented to combine the nearest two (or three) quarks into mesons (or baryons) [40]. The formed hadrons enter the subsequent hadronic rescattering process using a relativistic transport (ART) model [46], in which both elastic and inelastic scattering are considered for baryon-baryon, baryon-meson, and meson-meson interactions. The hadronic interaction time was set by default to $t_{max} = 30\,\text{fm}/c$. Alternatively, t_{max} is set to $0.4\,\text{fm}/c$ to effectively turn off the hadron scattering process while still considering the resonance decay [47] (see set "w/o hadron scat." in Table 1). In addition, the random orientation of the reaction plane was turned on and the shadowing effect was considered in this analysis.

2.2 Two-particle correlation and non-flow subtraction

The two-particle correlation (2PC) method is widely used to extract the flow signal in small collision systems because it can suppress the non-flow contribution from long-range jet correlations [26–28, 30, 48]. Similar to Eq. 1, the azimuthal correlation between two emission particles can be represented by N^{pairs} pairs of emitted particles (labeled as $C(\Delta\varphi)$) as a function of the relative angle $\Delta\varphi = \varphi^a - \varphi^b$ between particles a and b and expanded in the Fourier series as follows:

$$C(\Delta\varphi) = \frac{dN^{\text{pair}}}{d\Delta\varphi} \propto 1 + 2\sum_{n=1}^{\infty} V_{n\Delta}(p_T^a, p_T^b)\cos[n(\Delta\varphi)], \quad (3)$$

where $V_{n\Delta}$ refers to the two-particle n-th order harmonic. In a pure hydrodynamic scenario, because particle emissions are independent, $V_{n\Delta}(p_T^a, p_T^b)$ can be factorized into the product of a single-particle flow v_n^a and v_n^b:

$$V_{n\Delta}(p_T^a, p_T^b) = v_n(p_T^a)v_n(p_T^b). \quad (4)$$

Based on the factorization assumption, v_n of a single particle a can be obtained using the 3×2PC method, which was recently proposed by the PHENIX Collaboration [49]. This requires the formation of two-particle correlations between three groups of particles (labeled a, b and c) and the extraction of the flow coefficients for three combinations:

$$v_n(p_T^a) = \sqrt{\frac{V_{n\Delta}(p_T^a, p_T^b)V_{n\Delta}(p_T^a, p_T^c)}{V_{n\Delta}(p_T^b, p_T^c)}}. \quad (5)$$

In small-collision systems, two main types of non-flow contributions to the flow signal are the near-side jet and away-side jet (recoil jet) correlations. The former can be effectively removed by introducing a large rapidity gap between the trigger and associated particles during the construction of the correlations. Several methods have been developed to subtract the latter [50]. A traditional approach is to directly subtract the correlation function distribution obtained from low-multiplicity events [27, 30] from that obtained from high-multiplicity events. This method assumes that the yield and shape of dijets are identical for both collision types as follows:

$$\begin{aligned} C^{\text{HM}}(\Delta\varphi) - C^{\text{LM}}(\Delta\varphi) &\propto 1 + 2\sum_{n=1}^{\infty} V_{n\Delta}\cos[n(\Delta\varphi)] \\ &= a_0 + 2\sum_{n=1}^{\infty} a_n\cos[n(\Delta\varphi)], \end{aligned} \quad (6)$$

where $C^{\text{LM}}(\Delta\varphi)$ and $C^{\text{HM}}(\Delta\varphi)$ represent the correlation function distributions obtained for low- and high-multiplicity events, respectively. This method relies on the "zero yield at minimum" (ZYAM) hypothesis [27, 30] that a flat combinatoric component should be subtracted from the correlation function in low-multiplicity events. Therefore, the fit parameter a_2 is the absolute modulation in the subtracted correlation function distribution and characterizes the modulation relative to a baseline, assuming that such a modulation is not present in the low-multiplicity class below the baseline. In this case, the flow coefficient $V_{n\Delta}$ is calculated as

$$V_{n\Delta} = a_n/(a_0 + b), \quad (7)$$

where b is the baseline, estimated using the minimum correlation function for low-multiplicity events. However, the measurement of jet-like correlations in p–Pb collisions indicates that the dependence of the dijet yield on the particle multiplicity cannot be ignored. In this case, a new template fit method was developed by the ATLAS collaboration [51], where the correlation function distribution obtained in high-multiplicity events is assumed to result from the superposition of the distribution obtained in low-multiplicity events scaled up by a multiplicative factor F and a constant modulated by $\cos(n\Delta\varphi)$ for $n > 1$, as shown in

$$C(\Delta\varphi) = FC^{\rm LM}(\Delta\varphi) + G\left(1 + 2\sum_{n=1}^{3} V_{n\Delta}\cos(n\Delta\varphi)\right), \quad (8)$$

where G denotes the normalization factor that maintains the integral of $C(\Delta\varphi)$ equal to $C^{\rm HM}(\Delta\varphi)$. Furthermore, an improved template fitting method [52] developed in recent years was tested. It applies a correction procedure to the default template fit method by considering the multiplicity dependence of the remaining ridge in low-multiplicity events, as shown in

$$V_{n\Delta} = V_{n\Delta}(\text{tmp}) - \frac{FG^{\rm LM}}{G^{\rm HM}}(V^2_{n\Delta}(\text{tmp}) - V^2_{n\Delta}(\text{LM})), \quad (9)$$

where $V_{n\Delta}(\text{tmp})$ and $V^2_{n\Delta}(\text{LM})$ are obtained by using the default template method for high- and low-multiplicity events. All these non-flow subtraction methods are implemented in this study, and their different sensitivities to non-flow effect are also discussed.

3 Analysis procedures

To directly compare the AMPT calculations with the results from ALICE, we focused on the particles within the pseudorapidity range $|\eta| < 0.8$, aligning with the TPC acceptance in ALICE [53]. In the 3×2PC method, long-range correlations were constructed between the charged particles at mid-rapidity, forward rapidity ($2.5 < \eta < 4$), and backward rapidity ($-4 < \eta < -2.5$), that is, the central-forward correlation ($-4.8 < \Delta\eta < -1.7$), central-backward correlation ($1.7 < \Delta\eta < 4.8$), and backward-forward correlations ($-8 < \Delta\eta < -5$). In addition, the centrality classes are defined by counting the charged particles in the acceptance of the V0A detector [53], that is, $2.8 < \eta < 5.1$.

The correlation function distribution $C(\Delta\varphi)$ was obtained by correcting the number of particle pairs in the same events normalized to the number of trigger particles $N_{\rm trig}$ by using an event-mixing technique:

$$C(\Delta\varphi, \Delta\eta) = \frac{1}{N_{\rm trig}}\frac{{\rm d}^2N_{\rm pairs}}{{\rm d}\Delta\eta{\rm d}\Delta\varphi} = \frac{S(\Delta\varphi, \Delta\eta)}{B(\Delta\varphi, \Delta\eta)}, \quad (10)$$

where $S(\Delta\varphi, \Delta\eta) = \frac{1}{N_{\rm trig}}\frac{{\rm d}^2N_{\rm same}}{{\rm d}\Delta\eta{\rm d}\Delta\varphi}$ is the correlation function in same events and $B(\Delta\varphi, \Delta\eta) = \alpha\frac{{\rm d}^2N_{\rm mixed}}{{\rm d}\Delta\eta{\rm d}\Delta\varphi}$ is the associated yield as a function of $\Delta\varphi$ and $\Delta\varphi$ in mixed events. Factor α is used to normalize $B(\Delta\varphi, \Delta\eta)$ to unity in the $\Delta\eta$ region of the maximal pair acceptance. The obtained 2-D correlation function $C(\Delta\varphi, \Delta\eta)$ is projected onto $\Delta\varphi$ axis, and we follow the non-flow subtraction procedures and factorization, as discussed in Eqs. 5–9, v_2 of the charged particles at $|\eta| < 0.8$ can be calculated.

4 Results and discussion

We first investigated the $p_{\rm T}$ spectrum of the identified particles before performing the flow analysis. Figure 1 illustrates the $p_{\rm T}$ distribution of proton, pion, and kaon in 0–20% high-multiplicity p–Pb collisions at $\sqrt{s_{\rm NN}} = 5.02$ TeV, which are obtained from AMPT with three different sets of configurations listed in Table 1 and ALICE experimental data [54]. The AMPT results, both with and without hadronic rescattering, are consistent. This behavior differs from previous findings in heavy-ion collisions, where the hadronic interaction significantly reduces the particle yield [55]. The spectrum obtained in the AMPT without considering the parton cascade process is enhanced compared to that obtained with partonic scattering, and this enhancement is more significant at a high $p_{\rm T}$. This outcome is expected because partons experience energy loss during the parton cascade, which reduces the production of final-state particles. In addition, the ratios of the $p_{\rm T}$ spectra obtained from the AMPT calculations and data are shown. The AMPT model calculation reproduces the particle yields well at low and intermediate $p_{\rm T}$ values when both partonic and hadronic scattering are included; however, it overestimates the high $p_{\rm T}$ data because parton-parton inelastic collisions and, subsequently, hard parton fragmentation are absent in the model [42].

Figure 2 (left) shows the v_2 of pions, kaons, protons and Λ as a function of $p_{\rm T}$ in 0–20% high-multiplicity p–Pb collisions at $\sqrt{s_{\rm NN}} = 5.02$ TeV, obtained in AMPT calculations

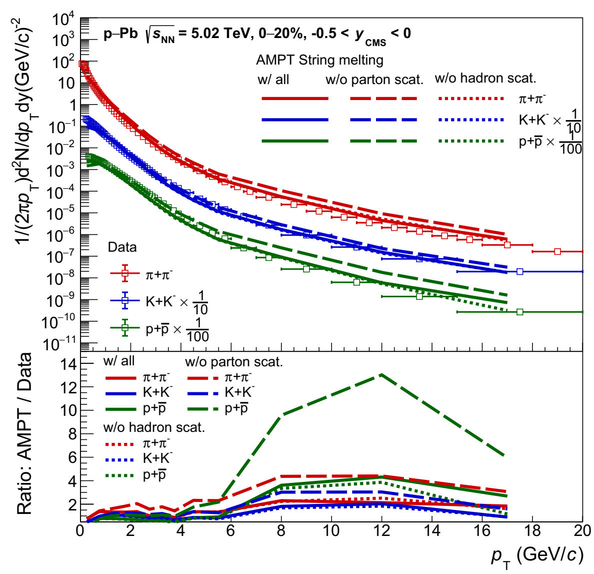

Fig. 1 (Color online) The $p_{\rm T}$ distribution of pions, kaons, and protons in 0–20% high-multiplicity p–Pb collisions at $\sqrt{s_{\rm NN}} = 5.02$ TeV, obtained from AMPT model calculations, is compared to ALICE measurement [54]. The results in AMPT without hadronic scattering and partonic scattering are also presented

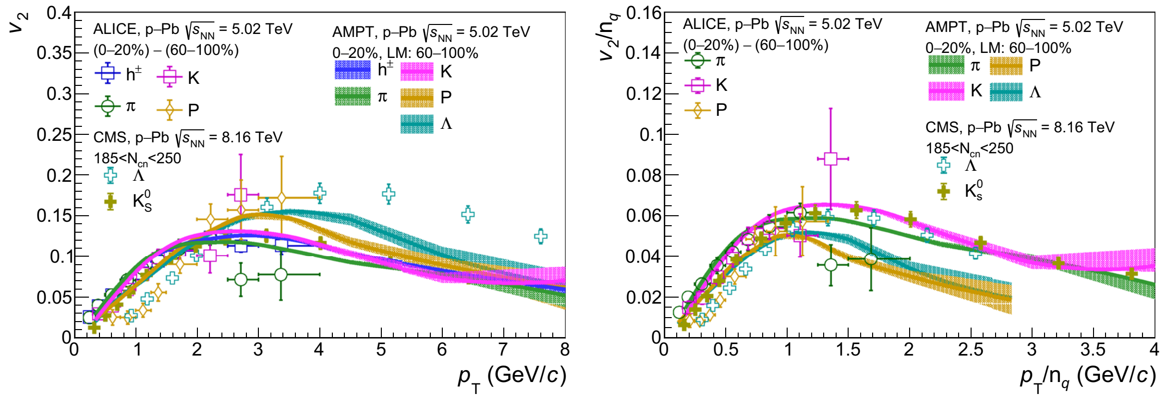

Fig. 2 (Color online) Left: the v_2 as a function of p_T in 0–20% high-multiplicity p–Pb collisions at $\sqrt{s_{NN}} = 5.02$ TeV, obtained from default AMPT model calculations with 3×2PC method, is compared to ALICE and CMS measurement [30, 31]. Right: the p_T-differential v_2 scaled by the number of constituent quark (n_q)

with 3×2PC method. A comparison with the ALICE measurement for v_2 of charged hadrons, pions, kaons, and protons [30] and the CMS measurement for v_2 of K^0_s and Λ [31] is also presented. The AMPT calculations applied the template fit method to suppress the away-side jet contribution and considered the ZYAM assumption to enable direct comparison with the observed data. The v_2 values of charged hadrons, pions, and kaons can be described well by AMPT calculations, but the v_2 values of baryons (protons and Λ) cannot be reproduced. In addition, the mass-ordering effect (i.e., the v_2 of baryons is lower than that of mesons) is reproduced for $p_T < 2$ GeV/c. Owing to the advanced flow extraction method, the calculations of v_2 were extended to the high-p_T region, up to 8 GeV/c in the AMPT model for the first time. The v_2 values of protons and Λ are consistent, and both of them are observed to have a higher value of v_2 value than that of the mesons for $2 < p_T < 7$ GeV/c. The observed meson-baryon particle type grouping in heavy-ion collision flow measurements indicates collective behavior at the partonic level, leading to the coalescence of quarks into hadrons. The number-of-constituent-quarks (NCQ) scaling techniques described in [22] can be used for further studies of this grouping. v_2 and p_T in Fig. 2 (left) are replaced by v_2/n_q and p_T/n_q, where the n_q is the number of constituent quark in mesons ($n_q = 2$) and baryons ($n_q = 3$), as shown in Fig. 2 (right). v_2/n_q obtained from the data show approximate values at intermediate p_T; however, the results calculated in AMPT cannot reproduce the scaling in $p_T/n_q > 1$ GeV/c. In order to consider the observed mass hierarchy of v_2, we also plot the v_2 of identified particle as a function of the transverse kinetic energy kE_T ($kE_T = m_T - m_0 = \sqrt{p_T^2 + m_0^2} - m_0$), and its NCQ scaling in Fig. 3 (left), and Fig. 3 (right). All particle species showed a set of similar v_2 values after NCQ scaling in $kE_T/n_q < 1$ GeV, confirming that the quark degree of freedom in flowing matter can also be probed in the transport model. However, this NCQ scaling is violated for $kE_T/n_q > 1$

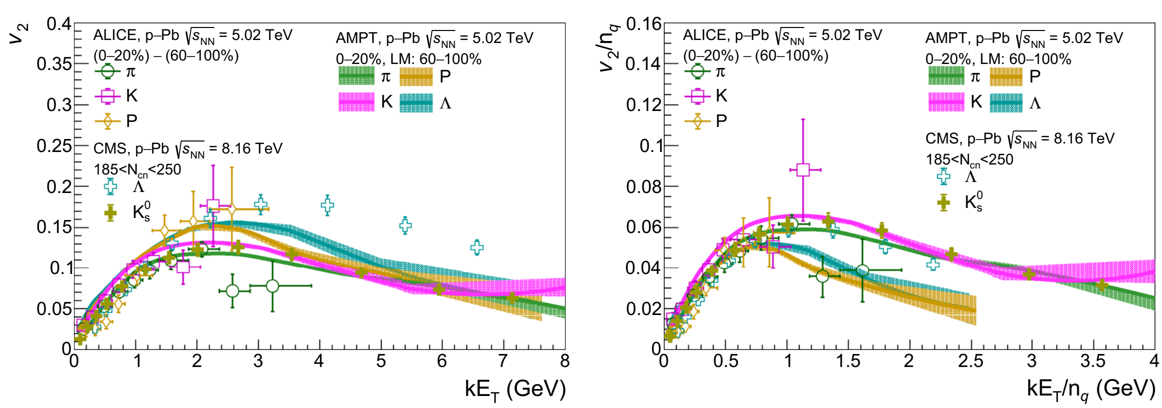

Fig. 3 (Color online) Left: the v_2 as a function of transverse kinetic energy (kE_T) in 0–20% high-multiplicity p–Pb collisions at $\sqrt{s_{NN}} = 5.02$ TeV, obtained from default AMPT model calculations with 3×2PC method, is compared to ALICE and CMS measurement [30, 31]. Right: the kE_T-differential v_2 scaled by the number of constituent quark (n_q)

GeV. This may be attributed to the hadronization mechanism implemented in the AMPT model used in this study, where baryons are produced only after the formation of mesons by simply combining the three nearest partons, regardless of the relative momentum among the coalescing partons. This results in an underestimation of the baryon v_2 at intermediate p_T in this study. An improved coalescence model implemented in the newer AMPT [56] introduced a new coalescence parameter to control the relative probability of a quark forming a baryon instead of a meson precisely. This improvement could have different NCQ scaling on v_2 but requires more systematic studies. Further studies on v_2 calculations in small collision systems with other improved hadronization mechanisms, for example, considering the Wigner function [57] and hard parton fragmentation [58], should be performed in the future.

We also extend our investigation to include a study of integrated v_2 within various centrality bins spanning the 0–60% range. We focus on the region where the NCQ scaling criterion is satisfied, that is, for transverse kinetic energies per constituent quark (kE_T/n_q) ranging from 0.4 to 1 GeV. The non-flow contribution was estimated and subtracted within the 60–100% centrality class by using the template fit method. As shown in Fig. 4, the v_2 values as a function of centrality exhibit a systematic decrease from central to peripheral collisions, reflecting the changing dynamic conditions and particle production mechanisms in different collision zones. Intriguingly, in the v_2 measurements, we observed a distinct mass-splitting phenomenon, with baryons and mesons exhibiting distinct elliptic flow patterns. Such a mass dependence in v_2 is similar to that in heavy-ion collisions at the LHC energies presented in a previous study [47]. This provides valuable insights into the collective behavior of different particle species within the evolving fireball created during these collisions.

Moreover, to gain a deeper understanding of the NCQ scaling properties, we explored the ratios of n_q-scaled integrated v_2 values for protons relative to pions and kaons relative to pions as functions of centrality. The results are shown in Fig. 5. A notable trend is observed in these ratios: they tend to approach unity as the collisions become more peripheral. It indicates that the collective flow of particles in low-multiplicity events may be approaching a behavior that is closer to the expected scaling behavior based on the number of constituent quark.

The effects of partonic and hadronic scattering on the elliptical anisotropy of the final-state particles were examined in this study. Figure 6 shows the calculated p_T-differential v_2 of pions, kaons, and protons in AMPT with

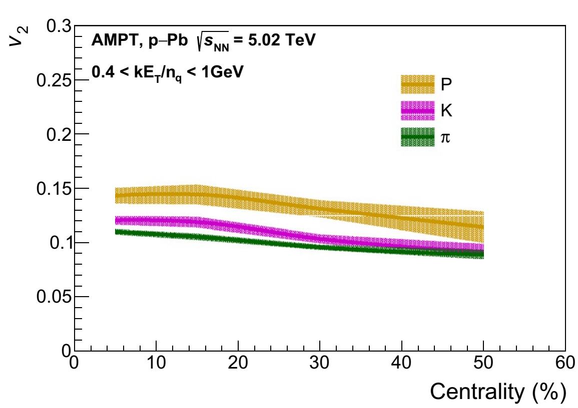

Fig. 4 (Color online) The integrated v_2 in 0.4 < kE_T/n_q <1 GeV for pion, kaon and proton varying with the centrality

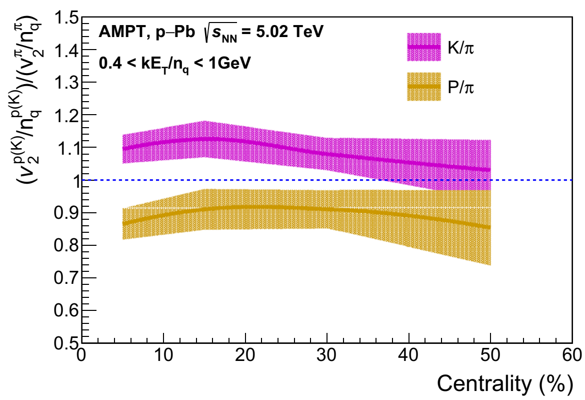

Fig. 5 (Color online) The ratio of integrated v_2 within 0.4< kE_T/n_q <1 GeV for proton over pion and kaon over pion varying with the centrality. The dash line represents the location of unity ratio

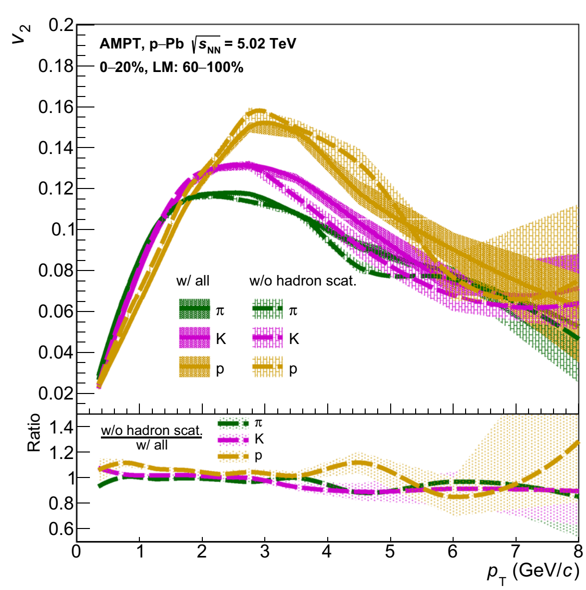

Fig. 6 (Color online) The p_T-differential v_2 of pions, kaons, and protons calculated in AMPT model with and without considering hadronic scattering. The ratios of the two sets are also presented

and without considering hadronic rescattering process in 0–20% high-multiplicity p-Pb collisions. The results show that the ratio of the v_2 values with and without hadronic rescattering is consistent with unity for all particle species, indicating that the hadronic rescattering mechanism has almost no effect on v_2 in high-multiplicity p–Pb collisions. We also investigated the centrality dependence of the hadronic rescattering effects by calculating p_{T}-integrated v_2 in several centrality bins between 0 and 60%, as illustrated in Fig. 7. The results demonstrate that the influence of hadronic rescattering is independent of the centrality selection and has almost no impact on NCQ scaling in the range of $0.4 < kE_{\mathrm{T}}/n_{\mathrm{q}} < 1$ GeV.

On the other hand, when we set the parton scattering cross section σ to zero but maintain the hadronic scatterings, the $V_{2\Delta}$ of charged particles for the central-forward (CF) and central-backward (CB) correlations is almost zero, as shown in Fig. 8. If both the partonic and hadronic scatterings are turned off, the results remain consistent with zero. This indicates that the elliptical anisotropy in high-multiplicity small-collision systems is mostly generated by parton scattering. Our conclusion is consistent with previous studies on the AMPT [41], which suggested that the majority of elliptic anisotropies comes from the anisotropic escape probability of partons.

Finally, different non-flow subtraction methods were investigated in this study. Figure 9 (left) shows the p_{T}-differential v_2 of the charged particles calculated using the 3×2PC method in 0–20% high-multiplicity p–Pb collisions.

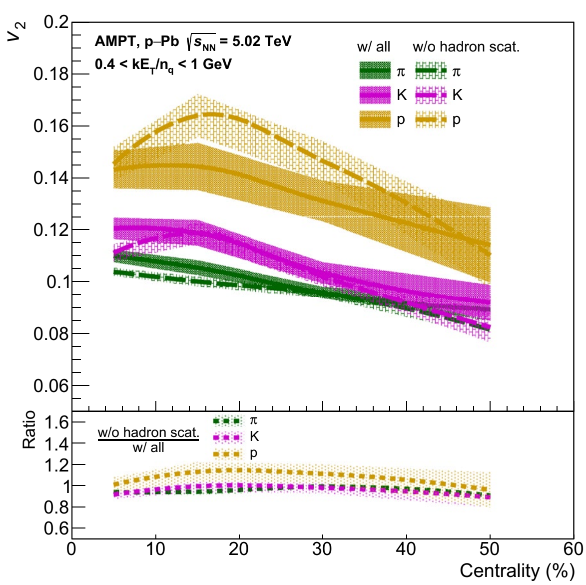

Fig. 7 (Color online) The integrated v_2 in $0.4 < kE_{\mathrm{T}}/n_q < 1$ GeV for pions, kaons, and protons calculated in AMPT model with and without considering hadronic scattering. The ratios of the two sets are also presented

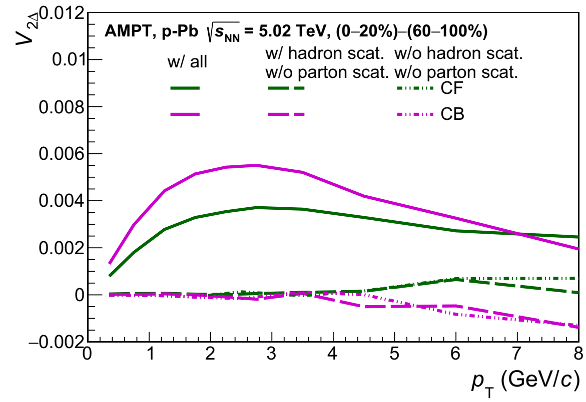

Fig. 8 (Color online) The p_{T}-differential $V_{2\Delta}$ for central-forward (CF) and central-backward (CB) correlations calculated in AMPT model with and without considering partonic scattering

Several non-flow subtraction methods are implemented. To demonstrate how the non-flow contribution is removed, v_2 obtained with a direct Fourier transform of the $C(\Delta\varphi)$ correlation (as shown in Eq. 3). The results show significant suppression across all the subtraction methods, particularly at higher p_{T} values where jet correlations are dominant. The results obtained with peripheral subtraction and template fitting were consistent, indicating that the away-side jet contribution was automatically removed using the 3×2PC method, even though the dependence of the jet correlation on multiplicity was not considered in the peripheral subtraction method. The v_2 calculated using the improved template fit method was slightly lower than that from the template fit, and it was similar to the features observed in the ATLAS measurement [52]. The same conclusions were drawn for the extraction of the identified particles (pions, kaons, protons, and Λ) v_2.

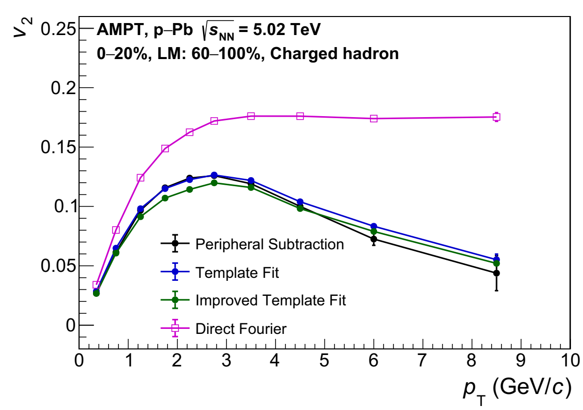

Fig. 9 (Color online) The p_{T}-differential v_2 of charged hadrons calculated in AMPT with different non-flow subtraction methods

5 Summary

This study systematically investigated the elliptic anisotropy of identified particles (pions, kaons, protons, and Λ) in p–Pb collisions at 5.02 TeV using the AMPT model. We extended the calculation of v_2 to higher p_T regions, up to 8 GeV/c, using advanced non-flow subtraction techniques for the first time. We also examined the mass-ordering effect and baryon-meson grouping at low and intermediate p_T, respectively. We argue that, with the approximate NCQ scaling of baryons and mesons, v_2 can be reproduced well at $kE_T/n_q < 1$ GeV for several centrality bins. Furthermore, we demonstrate that parton interactions can simultaneously decrease the yield of light hadrons and generate significant v_2. However, hadronic rescatterings had little influence on the elliptical anisotropy of the final-state particles. Thus, these findings indicate that the non-equilibrium anisotropic parton escape mechanism coupled with the quark coalescence model can also reproduce the hydro-like behavior of the identified particles observed in small collision systems. Overall, this study provides new insights into the existence of partonic collectivity in small collision systems.

Acknowledgements We would like to thank Guo-Liang Ma for the helpful discussions.

Author contributions All authors contributed to the study conception and design. Material preparation, data collection and analysis were performed by Si-Yu Tang, Liang Zheng, Xiao-Ming Zhang, and Ren-Zhuo Wan. The first draft of the manuscript was written by Si-Yu Tang, and all authors commented on previous versions of the manuscript. All authors read and approved the final manuscript.

Data availability The data that support the findings of this study are openly available in Science Data Bank at https://cstr.cn/31253.11.sciencedb.j00186.00382 and https://www.doi.org/10.57760/sciencedb.j00186.00382

Declarations

Conflict of interest The authors declare that they have no conflict of interest.

References

1. E.V. Shuryak, Quark-gluon plasma and hadronic production of leptons, photons and psions. Phys. Lett. B **78**, 150 (1978). https://doi.org/10.1016/0370-2693(78)90370-2
2. E.V. Shuryak, Quantum chromodynamics and the theory of superdense matter. Phys. Rept. **61**, 71–158 (1980). https://doi.org/10.1016/0370-1573(80)90105-2
3. J.Y. Ollitrault, Anisotropy as a signature of transverse collective flow. Phys. Rev. D **46**, 229–245 (1992). https://doi.org/10.1103/PhysRevD.46.229
4. S.A. Voloshin, Anisotropic collective phenomena in ultra-relativistic nuclear collisions. Nucl. Phys. A **827**, 377C-382C (2009). https://doi.org/10.1016/j.nuclphysa.2009.05.082
5. S. Voloshin, Y. Zhang, Flow study in relativistic nuclear collisions by Fourier expansion of Azimuthal particle distributions. Z. Phys. C **70**, 665–672 (1996). https://doi.org/10.1007/s002880050141
6. A.M. Poskanzer, S.A. Voloshin, Methods for analyzing anisotropic flow in relativistic nuclear collisions. Phys. Rev. C **58**, 1671–1678 (1998). https://doi.org/10.1103/PhysRevC.58.1671
7. B. Alver, G. Roland, Collision geometry fluctuations and triangular flow in heavy-ion collisions. Phys. Rev. C **81**, 054905 (2010). https://doi.org/10.1103/PhysRevC.81.054905
8. B.H. Alver, C. Gombeaud, M. Luzum et al., Triangular flow in hydrodynamics and transport theory. Phys. Rev. C **82**, 034913 (2010). https://doi.org/10.1103/PhysRevC.82.034913
9. G.-Y. Qin, H. Petersen, S.A. Bass et al., Translation of collision geometry fluctuations into momentum anisotropies in relativistic heavy-ion collisions. Phys. Rev. C **82**, 064903 (2010). https://doi.org/10.1103/PhysRevC.82.064903
10. D. Teaney, L. Yan, Triangularity and dipole asymmetry in heavy ion collisions. Phys. Rev. C **83**, 064904 (2011). https://doi.org/10.1103/PhysRevC.83.064904
11. I. Arsene, I.G. Bearden, D. Beavis et al., Quark gluon plasma and color glass condensate at RHIC? The perspective from the BRAHMS experiment. Nucl. Phys. A **757**, 1–27 (2005). https://doi.org/10.1016/j.nuclphysa.2005.02.130
12. K. Adcox, S.S. Adler, S. Afanasiev et al., Formation of dense partonic matter in relativistic nucleus-nucleus collisions at RHIC: experimental evaluation by the PHENIX collaboration. Nucl. Phys. A **757**, 184–283 (2005). https://doi.org/10.1016/j.nuclphysa.2005.03.086
13. B.B. Back, M.D. Baker, M. Ballintijn et al., The PHOBOS perspective on discoveries at RHIC. Nucl. Phys. A **757**, 28–101 (2005). https://doi.org/10.1016/j.nuclphysa.2005.03.084
14. J. Adams, M.M. Aggarwal, Z. Ahammed et al., Experimental and theoretical challenges in the search for the quark gluon plasma: the STAR Collaboration's critical assessment of the evidence from RHIC collisions. Nucl. Phys. A **757**, 102–183 (2015). https://doi.org/10.1016/j.nuclphysa.2005.03.085
15. K. Aamodt, B. Abelev, A.A. Quintana et al., Higher harmonic anisotropic flow measurements of charged particles in Pb–Pb collisions at $\sqrt{s_{NN}}$ =2.76 TeV. Phys. Rev. Lett. **107**, 032301 (2011). https://doi.org/10.1103/PhysRevLett.107.032301
16. S. Acharya, F.T. Acosta, D. Adamova et al., Energy dependence and fluctuations of anisotropic flow in Pb–Pb collisions at $\sqrt{s_{NN}}$ = 5.02 and 2.76 TeV. J. High Energy Phys. **07**, 103 (2018). https://doi.org/10.1007/JHEP07(2018)103
17. G. Aad, B. Abbott, J. Abdallah et al., Measurement of the azimuthal anisotropy for charged particle production in $\sqrt{s_{NN}}$ = 2.76 TeV lead-lead collisions with the ATLAS detector. Phys. Rev. C **86**, 014907 (2012). https://doi.org/10.1103/PhysRevC.86.014907
18. S. Chatrchyan, V. Khachatryan, A.M. Sirunyan et al., Measurement of higher-order harmonic azimuthal anisotropy in PbPb collisions at $\sqrt{s_{NN}}$ = 2.76 TeV. Phys. Rev. C **89**, 044906 (2014). https://doi.org/10.1103/PhysRevC.89.044906
19. S. Acharya, D. Adamova, A. Adler et al., Anisotropic flow and flow fluctuations of identified hadrons in Pb–Pb collisions at $\sqrt{s_{NN}}$ = 5.02 TeV. J. High Energy Phys. **05**, 243 (2023). https://doi.org/10.1007/JHEP05(2023)243
20. S. Acharya, D. Adamova, A. Adler et al., Anisotropic flow of identified hadrons in Xe–Xe collisions at $\sqrt{s_{NN}}$ = 5.44 TeV. J. High Energy Phys. **10**, 152 (2021). https://doi.org/10.1007/JHEP10(2021)152
21. Y.-G. Ma, The collective flow from the degree of freedom of nucleons to quarks. J. Fudan Univ. (Nat. Sci.) **62**, 273–292 (2023). https://doi.org/10.15943/j.cnki.fdxb-jns.20230525.001

22. D. Molnar, S.A. Voloshin, Elliptic flow at large transverse momenta from quark coalescence. Phys. Rev. Lett. **91**, 092301 (2003). https://doi.org/10.1103/PhysRevLett.91.092301
23. Z.-W. Lin, D. Molnar, Quark coalescence and elliptic flow of charm hadrons. Phys. Rev. C **68**, 044901 (2003). https://doi.org/10.1103/PhysRevC.68.044901
24. M. Wang, J.-Q. Tao, H. Zheng et al., Number-of-constituent-quark scaling of elliptic flow: a quantitative study. Nucl. Sci. Tech. **33**, 37 (2022). https://doi.org/10.1007/s41365-022-01019-9
25. T.-Z. Yan, Y.-G. Ma, X.-Z. Cai et al., Scaling of anisotropic flow and momentum-space densities for light particles in intermediate energy heavy ion collisions. Phys. Lett. B **638**, 50–54 (2006). https://doi.org/10.1016/j.physletb.2006.05.018
26. S. Chatrchyan, V. Khachatryan, A.M. Sirunyan et al., Observation of long-range near-side angular correlations in proton-lead collisions at the LHC. Phys. Lett. B **718**, 795–814 (2013). https://doi.org/10.1016/j.physletb.2012.11.025
27. B. Abelev, J. Adam, D. Adamova et al., Long-range angular correlations on the near and away side in p–Pb collisions at $\sqrt{s_{\rm NN}}$ = 5.02 TeV. Phys. Lett. B **719**, 29–41 (2013). https://doi.org/10.1016/j.physletb.2013.01.012
28. G. Aad, T. Abajyan, B. Abbott et al., Observation of associated near-side and away-side long-range correlations in $\sqrt{s_{\rm NN}}$ =5.02 TeV proton-lead collisions with the ATLAS detector. Phys. Rev. Lett. **110**, 182302 (2013). https://doi.org/10.1103/PhysRevLett.110.182302
29. M.I. Abdulhamid, B.E. Aboona, J. Adam et al., Measurements of the elliptic and triangular azimuthal anisotropies in central ^{3}He+Au, d+Au and p+Au collisions at $\sqrt{s_{\rm NN}}$ = 200 GeV. Phys. Rev. Lett. **130**, 242301 (2023). https://doi.org/10.1103/PhysRevLett.130.242301
30. B. Abelev, J. Adam, D. Adamova et al., Long-range angular correlations of π, K and p in p–Pb collisions at $\sqrt{s_{\rm NN}}$ = 5.02 TeV. Phys. Lett. B **726**, 164–177 (2013). https://doi.org/10.1016/j.physletb.2013.08.024
31. A.M. Sirunyan, A. Tumasyan, W. Adam et al., Elliptic flow of charm and strange hadrons in high-multiplicity pPb collisions at $\sqrt{s_{\rm NN}}$ = 8.16 TeV. Phys. Rev. Lett. **121**, 082301 (2018). https://doi.org/10.1103/PhysRevLett.121.082301
32. P. Bozek, Collective flow in p–Pb and d–Pd collisions at TeV energies. Phys. Rev. C **85**, 014911 (2012). https://doi.org/10.1103/PhysRevC.85.014911
33. P. Bozek, W. Broniowski, Correlations from hydrodynamic flow in p–Pb collisions. Phys. Lett. B **718**, 1557–1561 (2013). https://doi.org/10.1016/j.physletb.2012.12.051
34. J.L. Nagle, W.A. Zajc, Small system collectivity in relativistic hadronic and nuclear collisions. Ann. Rev. Nucl. Part. Sci. **68**, 211–235 (2018). https://doi.org/10.1146/annurev-nucl-101916-123209
35. G. Nijs, W. van der Schee, U. Gürsoy et al., Bayesian analysis of heavy ion collisions with the heavy ion computational framework Trajectum. Phys. Rev. C **103**, 054909 (2021). https://doi.org/10.1103/PhysRevC.103.054909
36. G. Nijs, W. van der Schee, U. Gürsoy et al., Transverse momentum differential global analysis of heavy-ion collisions. Phys. Rev. Lett. **126**, 202301 (2021). https://doi.org/10.1103/PhysRevLett.126.202301
37. W.-B. Zhao, C.-M. Ko, Y.-X. Liu et al., Probing the partonic degrees of freedom in high-multiplicity p-Pb collisions at $\sqrt{s_{\rm NN}}$ = 5.02 TeV. Phys. Rev. Lett. **125**, 072301 (2020). https://doi.org/10.1103/PhysRevLett.125.072301
38. K. Dusling, R. Venugopalan, Comparison of the color glass condensate to dihadron correlations in proton–proton and proton–nucleus collisions. Phys. Rev. D **87**, 094034 (2013). https://doi.org/10.1103/PhysRevD.87.094034
39. K. Dusling, R. Venugopalan, Evidence for BFKL and saturation dynamics from dihadron spectra at the LHC. Phys. Rev. D **87**, 051502 (2013). https://doi.org/10.1103/PhysRevD.87.051502
40. Z.-W. Lin, C.M. Ko, B.-A. Li et al., A multi-phase transport model for relativistic heavy ion collisions. Phys. Rev. C **72**, 064901 (2005). https://doi.org/10.1103/PhysRevC.72.064901
41. L. He, T. Edmonds, Z.-W. Lin et al., Anisotropic parton escape is the dominant source of azimuthal anisotropy in transport models. Phys. Lett. B **753**, 506–510 (2016). https://doi.org/10.1016/j.physletb.2015.12.051
42. Z.-W. Lin, L. Zheng, Further developments of a multi-phase transport model for relativistic nuclear collisions. Nucl. Sci. Tech. **32**, 113 (2021). https://doi.org/10.1007/s41365-021-00944-5
43. X.-N. Wang, M. Gyulassy, HIJING: a Monte Carlo model for multiple jet production in pp, pA and AA collisions. Phys. Rev. D **44**, 3501–3516 (1991). https://doi.org/10.1103/PhysRevD.44.3501
44. M. Gyulassy, X.-N. Wang, HIJING 1.0: A Monte Carlo program for parton and particle production in high-energy hadronic and nuclear collisions. Comput. Phys. Commun. **83**, 307 (1994). https://doi.org/10.1016/0010-4655(94)90057-4
45. B. Zhang, ZPC 1.0.1: A Parton cascade for ultrarelativistic heavy ion collisions. Comput. Phys. Commun. **109**, 193–206 (1998). https://doi.org/10.1016/S0010-4655(98)00010-1
46. B.-A. Li, C.M. Ko, Formation of superdense hadronic matter in high-energy heavy ion collisions. Phys. Rev. C **52**, 2037–2063 (1995). https://doi.org/10.1103/PhysRevC.52.2037
47. L. Zheng, H. Li, H. Qin et al., Investigating the NCQ scaling of elliptic flow at LHC with a multiphase transport model. Eur. Phys. J. A **53**, 124 (2017). https://doi.org/10.1140/epja/i2017-12312-8
48. Y.-G. Ma, W.-Q. Shen, Correlation functions and the disappearance of rotational collective motion in nucleus–nucleus collisions below 100 MeV/nucleon. Phys. Rev. C **51**, 3256–3263 (1995). https://doi.org/10.1103/PhysRevC.51.3256
49. N.J. Abdulameer, U. Acharya, A. Adare et al., Measurements of second-harmonic Fourier coefficients from azimuthal anisotropies in p+p, p+Au, d+Au, and ^{3}He+Au collisions at $\sqrt{s_{\rm NN}}$ = 200 GeV. Phys. Rev. C **107**, 024907 (2023). https://doi.org/10.1103/PhysRevC.107.024907
50. S.H. Lim, Q. Hu, R. Belmont et al., Examination of flow and nonflow factorization methods in small collision systems. Phys. Rev. C **100**, 024908 (2019). https://doi.org/10.1103/PhysRevC.100.024908
51. G. Aad, B. Abbott, J. Abdallah et al., Observation of long-range elliptic azimuthal anisotropies in $\sqrt{s}$ =13 and 2.76 TeV *pp* collisions with the ATLAS detector. Phys. Rev. Lett. **116**, 172301 (2016). https://doi.org/10.1103/PhysRevLett.116.172301
52. M. Aaboud, G. Aad, B. Abbott et al., Correlated long-range mixed-harmonic fluctuations measured in *pp*, *p*+Pb and low-multiplicity Pb+Pb collisions with the ATLAS detector. Phys. Lett. B **789**, 444–471 (2019). https://doi.org/10.1016/j.physletb.2018.11.065
53. B. Abelev, A. Abramyan, J. Adam et al., Performance of the ALICE experiment at the CERN LHC. Int. J. Mod. Phys. A **29**, 1430044 (2014). https://doi.org/10.1142/S0217751X14300440
54. J. Adam, D. Adamova, M.M. Aggarwa et al., Multiplicity dependence of charged pion, kaon, and (anti)proton production at large transverse momentum in p-Pb collisions at $\sqrt{s_{\rm NN}}$ = 5.02 TeV. Phys. Lett. B **760**, 720–735 (2016). https://doi.org/10.1016/j.physletb.2016.07.050
55. Z.-W. Lin, S. Pal, C.M. Ko et al., Charged particle rapidity distributions at relativistic energies. Phys. Rev. C **64**, 011902 (2001). https://doi.org/10.1103/PhysRevC.64.011902

56. Y.-C. He, Z.-W. Lin, Improved quark coalescence for a multi-phase transport model. Phys. Rev. C **96**, 014910 (2017). https://doi.org/10.1103/PhysRevC.96.014910
57. F.-T. Wang, J. Xu, Hadronization using the Wigner function approach for a multiphase transport model. Phys. Rev. C **100**, 064909 (2019). https://doi.org/10.1103/PhysRevC.100.064909
58. C. Zhang, L. Zheng, S.-S. Shi et al., Resolving the R_{pA} and v_2 puzzle of D^0 mesons in p−Pb collisions at the LHC. Phys. Lett. B **846**, 138219 (2023). https://doi.org/10.1016/j.physletb.2023.138219

Springer Nature or its licensor (e.g. a society or other partner) holds exclusive rights to this article under a publishing agreement with the author(s) or other rightsholder(s); author self-archiving of the accepted manuscript version of this article is solely governed by the terms of such publishing agreement and applicable law.